A NEW METHOD FOR STUDYING STRESS-INDUCED MICROCRACKS IN CONCRETE

By Kamran M. Nemati,[1] Fellow, ASCE, Paulo J. M. Monteiro,[2] and Neville G. W. Cook[3]

ABSTRACT: The experimental technique described below makes it possible to preserve the compressive stress-induced microcracks in concrete as they exist under applied loads. The results can be used to better understand and quantify the general relationship between stress level and crack development, as well as the effect of confinement on crack behavior. Also, it allows observations into the way small cracks are formed and then propagate in concrete, thereby making the application of fracture mechanics to concrete more accurate. Cylindrical specimens of concrete were subjected to testing under uniaxial and confined compression utilizing special testing equipment designed and developed specifically for this experimental study. An alloy with a low melting point was used as a pore fluid. At a specific stress, this alloy was solidified to preserve the stress-induced microcracks as they exist under load. Scanning electron microscopy was employed to capture images from the cross sections of normal and high-strength concrete specimens.

INTRODUCTION

Identifying cracks induced by loading and preserving these stress-induced microcracks are key to understanding the mechanisms for their formation, propagation, and interaction. To understand the mechanisms of crack formation, we must first examine the basic structure of concrete. Examining a cross section of concrete reveals two distinct entities: aggregate particles of varying size and shape and the binding medium that is composed of an incoherent mass of hydrated cement paste. At the microscopic level, it is obvious that these two entities are neither homogeneously distributed with respect to each other nor homogeneous themselves. The structure of hydrated cement paste in the vicinity of large and fine aggregate particles is usually very different from the structure of bulk paste. Therefore, in order to study the structural behavior of concrete, this complex mass must be viewed as a three-phase composite structure: a cement paste phase, bonded to the aggregate phase; and a transition zone, which represents the interfacial region between the particles of coarse and fine aggregates and the hydrated cement paste.

The investigation of microcracks in concrete ranges from a macroscopic study of the behavior of cracked specimens to a microscopic study of the cracks themselves. Several methods have been used to study the microcracking of concrete, including acoustic emission (Jones 1952; L'Hermite 1954; Hamstad 1986; Maji et al. 1990; Ouyang et al. 1991), sonic testing (Whitehurst 1966; Monteiro and King 1988), microscope technique with dye (Slate and Olsefski 1963; Hsu et al. 1963), mercury intrusion porosimetry (Orr 1969), X-ray technique (Buyukozturk et al. 1971, 1972; Liu et al. 1972; Carino and Slate 1976), computerized tomography analysis (Martz et al. 1993), and holographic interferometry (Mobasher et al. 1990; Maji and Shah 1990; Regnault et al. 1990). Almost all of the above-mentioned techniques have limited capability in accurately representing the geometry and state of microcracks as they exist under load. Many of the techniques are limited in their resolution, sensitivity in detecting cracks, and ability to

make full-field observations. Other methods are incapable of examining the specimen while under load or they require special preparation of the specimen, which alters its behavior.

The method described here involves the application of a metal in the liquid phase. Wood's metal, which has a melting point below the boiling point of water, preserves the microstructure of stress-induced microcracks in concrete as they exist under load (Nemati 1994; Scrivener and Nemati 1996; Nemati et al. 1998). Used in conjunction with scanning electron microscopy (SEM), it allows for detailed observation of compressive stress-induced microcracks in concrete. Used in the past few years to study the microstructure of different materials, Yadev (1984) used Wood's metal to study porosimetry and measure contact areas and voids between the surfaces of natural fractures, while Pyrak (1988) used Wood's metal to study the fracture of rocks. Zheng (1989) used Wood's metal to fill voids and microcracks in clastic rock specimens during loading and solidified it before unloading to preserve the microstructure in specimens under load.

The experimental technique described below makes it possible to preserve the compressive stress-induced microcracks in concrete as they exist under applied loads. The results of these experiments can be used to better understand and quantify the general relationship between stress level and crack development, as well as the effects of confinement on crack behavior, for example, crack orientation, crack density, crack length, crack localization, crack branching, and interfacial cracks. In addition, the results will facilitate investigations into the way small cracks form and then propagate in concrete, thus making the application of fracture mechanics to cement paste and concrete more accurate. Special test equipment, whereby a molten metal was injected into the cracks and allowed to solidify before unloading the specimen, was created to preserve the cracks under applied load.

TEST METHOD

The experiments carried out involved three procedures: (i) concrete casting and preparation, (ii) crack induction, and (iii) molten metal injection and solidification. The second and third procedures were carried out simultaneously. In order to preserve the microstructure and microcracks in concrete specimens under load, the voids and microcracks were filled with a liquid metal alloy called Wood's metal during loading, and the alloy was allowed to solidify in place before unloading the specimen. Wood's metal is a fusible alloy—which in the liquid phase is nonwetting—with an effective surface tension of about 400 mN/m (Yadev et al. 1984), a Young modulus of 9.7 GPa, and a density of 9.4 g/cm^3. It consists of 42.5% bismuth (Bi), 37.7% lead (Pb), 11.3% tin (Sn), and 8.5% cadmium

(Cd). It has a melting point range from 70°C to 88°C and is solid at room temperature. The advantage of Wood's metal is that it can be injected into voids and stress-induced microcracks at the desired stress level, then solidified at any stage of the experiment to preserve—in three-dimensional form—the geometry of the microcracks as they occur at any given stage of the experiment.

The lateral confining stress used to generate triaxial compression was supplied by stainless steel wires, 0.3 mm in diameter, that were wound around the concrete cylinders, both the entire length (fully confined) and one-third of the way from each end (partially confined), at a pretension of 670 N. The purpose of the partially confined test was to observe the extensile microcracks generated under uniaxial compression in the middle of the concrete cylinder without causing unstable failure of the entire cylinder. Because no failure occurred within the confined ends, the triaxial compression test also eliminated the end effect caused by friction between the loading plates and the ends of the concrete cylinder. In specimens subjected to uniaxial compression, most microcracks propagate to a certain length and stop. With the application of confining stress, however, the average length of the microcracks decreases. The stress intensity factor is a fundamental quantity that governs the stress field near the crack tip. The propagation of microcracks is controlled by the stress intensity factor at the microcrack tips, resulting from both local tensions (which generate the microcracks) and the overall stress field. The confining stress, which is orthogonal to the direction of maximum compression, adds a negative stress intensity factor, which stops the propagation of the extensile microcracks.

During the test, cylindrical concrete specimens were submerged in the molten metal alloy, and the alloy was driven into voids and fractures by pore pressure provided by nitrogen gas. The alloy can be solidified at any stage of the experiment to preserve the geometry of microcracks as they exist under load. With a surface tension of 400 mN/m, the alloy can penetrate into flat cracks with apertures as fine as 0.08 μm under a pore pressure of 10.3 MPa. This technique allows the observation of the geometry of the microcracks induced at any given stage of the experiment. The alloy is injected into voids and stress-induced microcracks at the desired stress level and then solidified at any stage of the experiment, preserving the microcracks three-dimensionally. After the metal solidified, each of the cylinders was sectioned into eight specimens. The specimens were examined using optical microscope and SEM.

Normal- and high-strength concrete cylinders 203 mm long and 102 mm in diameter were cast for this study. The cylinders were cured in 100% humidity at a temperature of 23°C.

TEST EQUIPMENT

The equipment used for this study, which consisted of a pedestal, a vessel, a piston, a top cap, and a heater, is described and illustrated below.

Pedestal

Made of graphatized steel, the pedestal is a monotonic, solid cylinder with a circular plate whose diameter is greater at the middle, as shown in Fig. 1. The cylinder is 127 mm long and 108 mm in diameter, except for the upper 25 mm, which has a diameter of 102 mm. The circular plate has a thickness of 25 mm and a diameter of 184 mm. The vessel is placed on the circular plate. An O-ring groove on the cylinder above the circular plate provides a fluid seal. There are six equally spaced 12.7 mm through holes on the circular plate to accommodate bolts that secure the vessel to the pedestal.
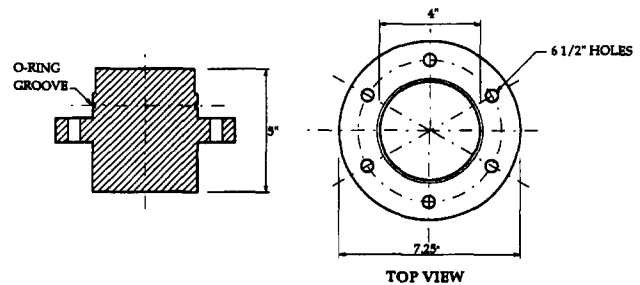

FIG. 1. Pedestal

Vessel

Made of high-strength steel, the vessel is a 298 mm tall, hollow cylinder with an outside diameter of 184 mm and an inside diameter of 108 mm. The diameter was enlarged to 133 mm at the top to provide a reservoir for the molten metal alloy at the time of testing. There are six 38 mm deep bolt holes with a diameter of 12.7 mm on the top and bottom of the vessel in order to secure the pedestal and the top cap to the vessel. Close to the top of the vessel, there is a 45°, 3 mm diameter hole with a plug at the end of it in order to facilitate the vacuum and nitrogen connection to the airtight assembly (Fig. 2). To prevent clogging, the hole is inclined to allow the Wood's metal to drain into the reservoir should the molten metal freeze because of a premature drop in temperature or if some other problem should occur while the experiment is in progress.

Piston

Made of high-strength steel, the piston is a 102 mm diameter, 127 mm tall solid cylinder that is placed on top of the concrete specimen and surrounded by the top cap. The piston transfers the applied compressive stresses from the loading machine to the concrete specimen (Fig. 3).

Top Cap

Made of galvanized steel, the top cap is a hollow, donut-shaped cylinder with two tiers and an inner radius of 102 mm.
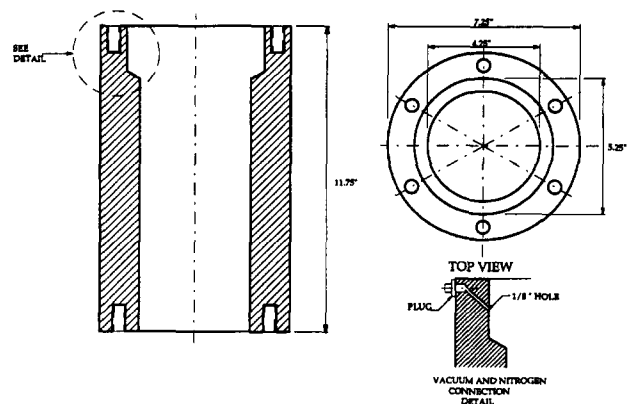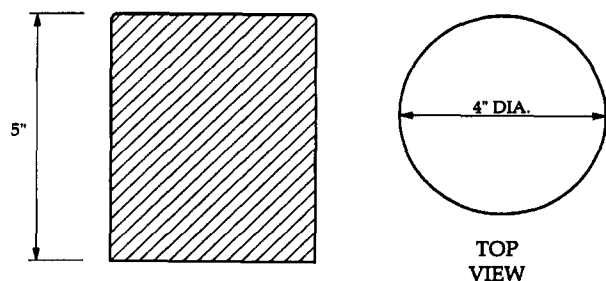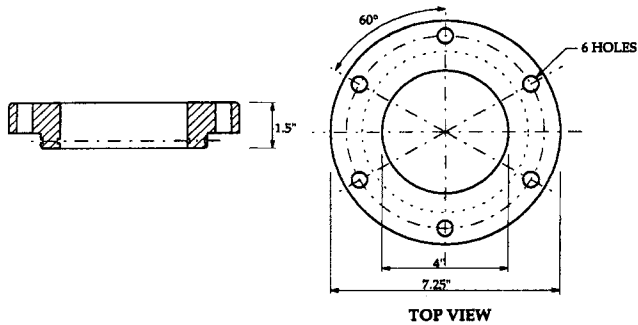

FIG. 2. Vessel

FIG. 3. Piston

FIG. 4. Top Cap

The top tier is 25 mm thick and has an outer radius of 184 mm. The bottom tier is 12.7 mm thick and has an outer radius of 133 mm. As with the pedestal, there are six equally spaced 12.7 mm through holes on the upper tier of the top cap to accommodate the bolts that secure it to the vessel. There are also two O-ring grooves on the inner and outer faces of the bottom tier (Fig. 4). Once assembled, the concrete cylinder rests on the pedestal, the top cap is closed, and the plug is connected to either vacuum or nitrogen. The entire system is airtight.

Heater

Heat was supplied by a ceramic heater operated by a microprocessor-based ramping temperature control unit. The ceramic heater was assembled inside two stainless steel half-cylinders with a 457 mm outside diameter and a 305 mm inside diameter. The half-cylinders were hinged together on one side and could be made into a monotonic unit by nuts and bolts on the other side.

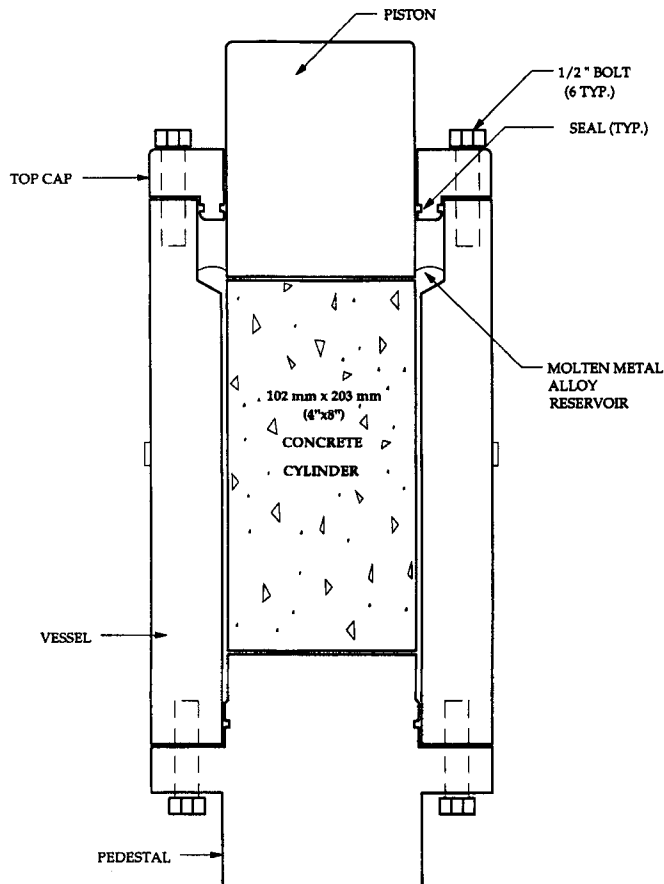Fig. 5 shows a schematic diagram of the test apparatus.

FIG. 5.   Diagram of Test Apparatus

EXPERIMENTAL PROCEDURE

Two different loading conditions, uniaxial and triaxial, were used to induce cracks in the concrete cylinders. Triaxiality was provided by the pretensioned wire wound around the concrete cylinders.

After preparation for testing, each concrete cylinder was first dried in an oven at a temperature of 43°C. This removed the moisture in the concrete and preheated the cylinder, ensuring that the molten metal alloy could penetrate into pores and cracks deep within its core without solidifying prematurely. The concrete cylinder was then placed on the pedestal inside the vessel and the piston was placed on top of it. The top cap was left open resting on three wedges a short distance from the top of the vessel so that the molten metal could be poured through the gap using a funnel [Fig. 6(a)]. At this point, a minimum load 0.7 MPa was applied to the piston to prevent the cylinder from floating after the Wood's metal was poured in. Once the concrete cylinder was submerged in the molten metal, the top cap was dropped by removing the wedges and then bolted tightly to the vessel. To monitor the temperature, a feedback thermocouple was inserted into a predrilled hole on the top cap [Fig. 6(b)]. To ensure uniform heating of the test assembly, a ceramic heater was then placed around the assembled system with a special noncombustible board placed on top to prevent heat convection. A linear variable displacement transducer (LVDT) for the axial displacement measurement was attached to the loading frame.

Heat was supplied in three stages. Starting at room temperature, the heat was then ramped up to 50°C and held at that temperature for 10 min; then the temperature was ramped up to 75°C and held there for an additional 10 min. The final stage involved ramping the temperature up to a target of 96°C
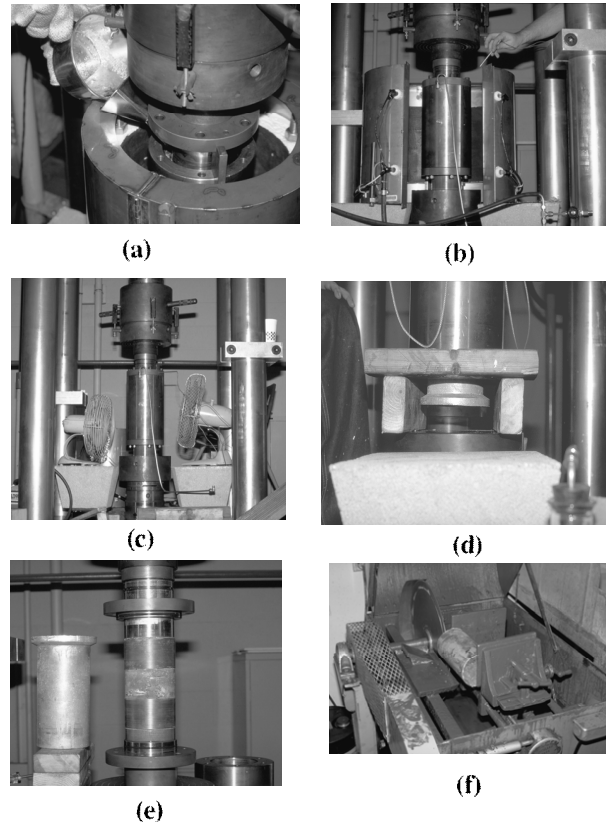

FIG. 6.   Various Stages of Experiment: (a) Pouring Molten Metal Into Vessel; (b) Inserting the Thermocouple Into the Top Cap; (c) Postexperiment Cooling of the Cell; (d) Extrusion of Concrete Specimen; (e) Specimen Prior to (Right) and after (Left) Injection of Wood's Metal; (f) Cutting the Concrete Cylinder after Molten Metal Injection
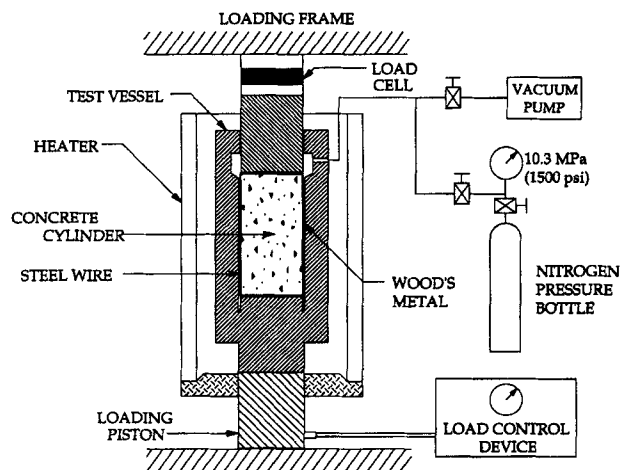
FIG. 7. Schematic Diagram of Test Assembly

for a period of 15 min and holding it at that temperature until the heat was no longer needed.

When the internal temperature reached at 96°C, a vacuum was applied to the vessel and kept constant for at least 30 min. The vacuum removed any air that might have become trapped in the concrete cylinder when it was assembled inside the vessel. The vacuum was removed after the desired axial stress level was applied.

Finally, in order to saturate the induced microcracks with the molten metal, nitrogen pressure was applied to the top of the vessel above the liquid Wood's metal. Controlled by a high-pressure regulator, 10.3 MPa of nitrogen was applied to the molten metal as the pore pressure; this pressure was kept constant throughout the tests and did not alter the effective stresses on the concrete cylinder. A surface tension of 400 mN/m allowed the alloy to penetrate into flat cracks with apertures as fine as 0.08 μm.

Throughout the period of loading and unloading, the axial load and the axial displacement were recorded on a data acquisition system and monitored on an x-y plotter. The axial stress point of interest was kept constant for 2 h to allow the liquid metal to penetrate into pores and fractures. Afterwards, fans were used to cool the vessel down to room temperature and to expedite solidification [Fig. 6(c)]. Approximately 3 h elapsed between the time pore pressure was applied and the period during which the metal was allowed to solidify. Finally, the specimen was extruded out of vessel for sectioning and SEM observation [Fig. 6(d)]. Fig. 6 illustrates different aspects of the experiment.

Fig. 7 shows a schematic diagram of the test assembly.

SPECIMEN PROCESSING FOR MICROSCOPIC ANALYSIS

After each experiment, the 102 by 203 mm concrete cylinder was sectioned along its long axis, using oil to cool the cutting saw [Fig. 6(f)]. An axial slab, approximately 5 mm thick, was sliced parallel to the direction of the load.

The concrete specimens extracted from the axial slab were 25 mm square and were approximately 5 mm thick. First, one side of each specimen was polished with 120, 220, 320, and 600 silicon carbide using a rotating grinder and mounting it against a 25 mm diameter glass plate with epoxy. In order to make both sides of the specimen parallel to each other, the samples were cut 2–3 mm thick by using a diamond slicing wheel with a nonaqueous lubricant (propylene glycol coolant). The specimens were then lapped (grinding on a flat surface) with a wheel grinder and polished with 600 silicon carbide. Further polishing was performed with 100-, 50-, and 10-μm aluminum powder on a glass plate. The final stage involved

treating specimens with 5-, 3-, and 0.25-μm diamond paste using special polishing equipment (ASTM 1993). After each stage of polishing, the specimens were immersed in acetone and placed in an ultrasonic machine in order to remove the residual silica film on their surfaces.

The acid etching technique makes it possible to observe three-dimensional microcracks in concrete with apertures as small as 0.08 μm. With this method specimens are submerged in 1 molar hydrochloric acid (HCl) solution for 20 min. The concrete surface is etched away, leaving a skeleton of metal alloy network on top of the new surface representing fractures and voids under load (Nemati and Monteiro 1997).

EXAMPLES OF APPLICATION

SEM was used to acquire images from the specimens. No stress-induced microcracks were observed in a reference specimen subjected to only a small compressive stress when filled with molten metal at a nitrogen pressure of 10.3 MPa. Fig. 8 shows a micrograph from the no-load experiment where the concrete is inherently cracked even before the application of any load (Hsu et al. 1963). These preload cracks are due to factors such as bleeding and drying shrinkage.

The specimens subjected to compressive loading were loaded to about 80%–85% of their ultimate strength. The microcracks in the loaded specimens were generated by several different mechanisms. Fig. 9 shows a micrograph taken from a specimen that was under uniaxial compression in the central portion, with the ends constrained by pretensioned wire, and a pore pressure of 10.3 MPa. As can be seen, microcracks
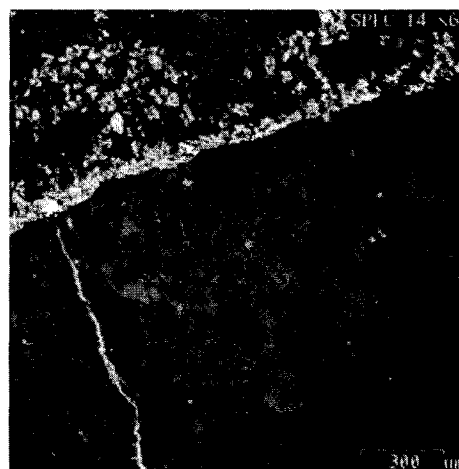

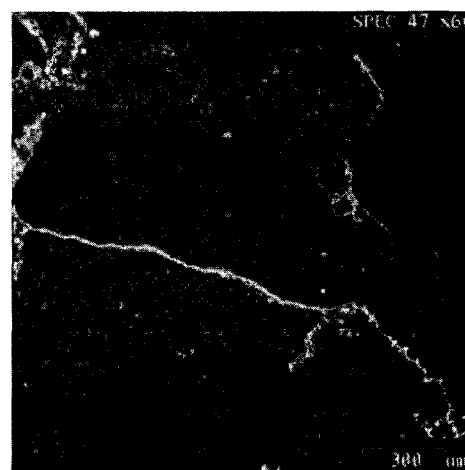FIG. 8. SEM Micrograph from No-Load Experiment

FIG. 9. SEM Micrograph from Partially Confined Experiment

propagated through the cement paste and along the transition zone. In comparison with Fig. 8, where there are no stress-induced microcracks, Fig. 9 clearly shows the generated microcracks as a result of axial loading.

Many cracks were generated from voids. Fig. 10 shows microcracks generated from a pore space that is filled with Wood's metal. These microcracks were generated as a result of local tensile stress tangential to the boundary of voids, with
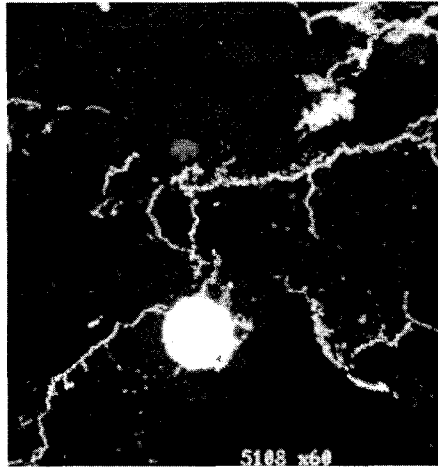
a value that was of the order of the maximum applied principal stress. It was found that these cracks usually started from the pore boundaries and then propagated in the direction of maximum compression.

Microcracks were also found to have been generated from the inside of aggregates, in a manner similar to a splitting tension test when the aggregates were loaded across their height. Fig. 11 shows a micrograph of this phenomenon for the uniaxial loading condition.

High-strength concrete behaves more like a homogeneous material than does normal-strength concrete. The stress-strain curves for high-strength concrete are steeper and closer to linearity to a high stress-strength ratio than in normal-strength concretes. This is due to a decrease in the amount and extent of microcracking in the transition zone. Thus, high-strength concrete exhibits a more brittle mode of fracture and less volumetric dilation (Carrasquillo et al. 1981) and has a stronger

FIG. 10. SEM Micrograph of Microcracks Propagating from a Pore
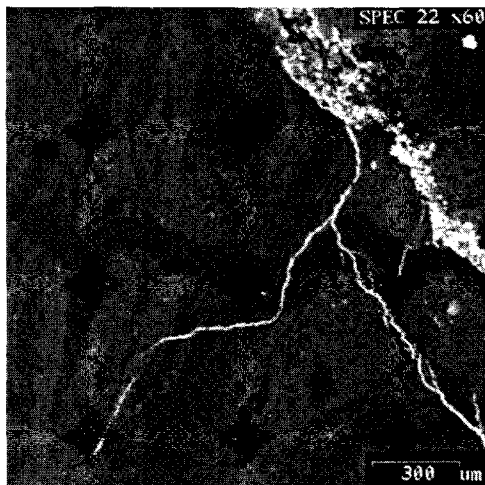
FIG. 11. SEM Micrograph of Aggregate Cracking

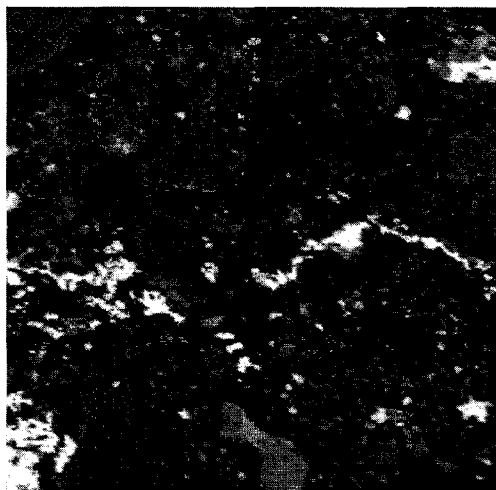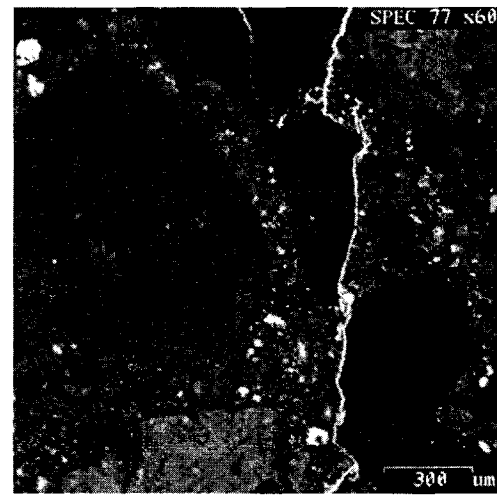FIG. 13. SEM Micrograph from Partially Confined Experiment for High-Strength Concrete

FIG. 14. Three-Dimensional Cracks

FIG. 12. SEM Micrograph from No-Load Experiment for High-Strength Concrete Specimen
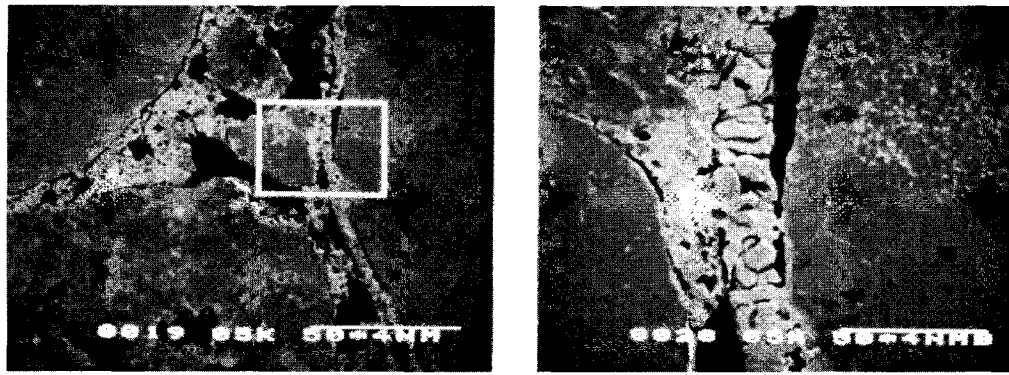

FIG. 15. Pore in Concrete

FIG. 16. Transition Zone Microcracks around the Aggregate Particles

and tougher cement paste owing to a lower water/cement ratio, resulting in a closer packing of cement grains and a reduced amount of pores and cracks. Apart from this microstructurally improved matrix, high-strength concrete also has a stronger transition zone. This presumably results from the reduction of excess bleeding and the filling of gaps by mineral admixtures, which in this case was rice husk ash. The microstructural differences between high-strength and normal-strength concrete cause significant differences in their deformation and fracture behavior. For example, high-strength concrete tends to behave with greater linear elasticity up to its peak strength, while normal-strength concrete typically exhibits nonlinear behavior, possibly because of interfacial crack extension prior to peak strength (Carrasquillo et al. 1981; Huang et al. 1989; ACI 1984). Furthermore, fracture development in high-strength concrete is usually accompanied by a relatively small process zone and tends to be characterized better by linear elastic fracture mechanics than does normal-strength concrete (Gettu et al. 1990).

Fig. 12 shows an SEM micrograph from the high-strength concrete specimen not under load. No stress-induced microcracks were observed in the reference specimen. The microcracks observed in these micrographs are attributed to factors such as drying shrinkage and specimen preparation. Fig. 13 shows an SEM micrograph of high-strength concrete conducted under a partially confining condition, that is, uniaxial compression in the central portion with ends constrained by pretensioned wire and a pore pressure of 10.3 MPa.

Clearly, less cracking occurred in high-strength than in normal-strength concrete, because of the stronger cement paste, with most of this cracking taking place in the transition zone. As high-strength concrete is more brittle, fracture in high-strength concrete is associated with less branching than in normal-strength concrete.

Three-dimensional observation of microstructure is possible by dissolving the cementious portion of the concrete specimens in 1 molar hydrochloric acid. Figs. 14–16 show micrographs taken using a scanning electron microscope after etching the specimens, which reveal the three-dimensional network of metal-filled fractures and voids.

CONCLUSIONS

Special testing equipment and an experimental technique have been developed that make possible the preservation of the compressive stress-induced microcracks in concrete as they exist under applied loads. This technique involved injecting a molten-metal alloy into the induced cracks and solidifying it before unloading.

SEM studies showed that, in the specimens subjected to no load, the interfacial transition zone is mostly a collection of interconnected pores. Once the load is applied, these pores connect to form microcracks, and they propagate to bridge the

microcracks generated in the cement paste matrix. The continuous crack pattern is thus formed. In high-strength concrete, where the strength of cement paste matrix is greatly improved, there was less interfacial porosity and also less crack interaction in the matrix. As high-strength concrete is more brittle, fracture in high-strength concrete is associated with less branching than in normal-strength concrete.

Dissolving the cementitious portion of the concrete specimens in acid allowed three-dimensional observation of microstructure, void structure, and the resulting stress-induced fractures. This method revealed useful information on transition zone microcracking, porosity, fracture planes, and crack interaction.

The molten-metal-injection technique used in this research is an efficient, cost-effective, and reliable method for the preservation of microcracks in concrete as they exist under load.

APPENDIX. REFERENCES

ACI Committee 363. (1984). "State of the art report on high strength concrete." *ACI J.*, 81(4), 364–411.

Buyukozturk, O., Nilson, A. H., and Slate, F. O. (1971). "Stress-strain response and fracture of concrete model in biaxial loading." *J. ACI, Proc.*, 68(5), 590–599.

Buyukozturk, O., Nilson, A. H., and Slate, F. O. (1972). "Deformation and fracture of a particulate composite." *J. Engrg. Mech. Div.*, ASCE, 98(3), 581–593.

Carino, N. J., and Slate, F. O. (1976). "Limiting tensile strain criterion for failure of concrete." *J. ACI, Proc.*, 73, 160–165.

Carrasquillo, R. L., Nilson, A. H., and Slate, F. O. (1981). "Properties of high strength concrete subject to short-term loads." *ACI J.*, 78(3), 171–178.

Gettu, R., Bazant, Z. P., and Karr, M. E. (1990). "Fracture properties and brittleness of high strength concrete." *ACI Mat. J.*, 87(6), 608–618.

Hamstad, M. A. (1986). "A review: Acoustic emission, a tool for composite materials studies." *Experimental Mech.*, 26(1), 7–13.

Hsu, T. T. C., Slate, F. O., Sturman, G. M., and Winter, G. (1963). "Microcracking of plain concrete and the shape of the stress-strain curve." *J. ACI, Proc.*, 60(14), 209–224.

Huang, J., and Li, V. C. (1989). "A meso-mechanical model of the tensile behavior of concrete—Part I: Modelling of pre-peak stress-strain relation." *Composites*, 20(4), 361–369.

Jones, R. (1952). "A method of studying the formation of cracks in a material subject to stresses." *British J. Appl. Phys.*, London, U.K., 229–232.

L'Hermite, R. (1954). "Present day ideas in concrete technology—Part 3: The failure of concrete." *RILEM Bull.*, 27–38.

Liu, T. C. Y., Nilson, A. H., and Slate, F. O. (1972). "Stress-strain response and fracture of concrete in uniaxial and biaxial compression." *J. ACI, Proc.*, 69(5), 291–295.

Maji, A. K., Ouyang, C., and Shah, S. P. (1990). "Fracture mechanics of quasi-brittle materials based on acoustic emission." *J. Mat. Res.*, 5(1), 206–217.

Maji, A. K., and Shah, S. P. (1990). "Measurement of mixed-mode crack profiles by holographic interferometry." *Experimental Mech.*, 30(2), 201–207.

Martz, H. E., Schneberk, D. J., Roberson, G. P., and Monteiro, P. J. M. (1993). "Computerized tomography analysis of reinforced concrete." *ACI Mat. J.*, 90(3), 259–264.

Mobasher, B., Castro-Montero, A., and Shah, S. P. (1990). "A study of fracture in fiber-reinforced cement-based composites using laser holographic interferometry." *Experimental Mech.*, 30(3), 201–207.

Monteiro, P. J. M., and King, M. S. (1988). "Experimental studies of elastic wave propagation in high-strength mortar." *ASTM J., Cement, Concrete, and Aggregates*, 10(2), 68–74.

Nemati, K. M. (1994). "Generation and interaction of compressive stress-induced microcracks in concrete," PhD thesis, Dept. of Civ. Engrg., Univ. of California at Berkeley.

Nemati, K. M., and Monteiro, P. J. M. (1997). "A new method to observe three-dimensional fractures in concrete using liquid metal prosimetry technique." *Cement and Concrete Res.*, 27(9), 1333–1341.

Nemati, K. M., Monteiro, P. J. M., and Scrivener, K. L. (1998). "Analysis of compressive stress-induced cracks in concrete." *ACI Mat. J.*, in press.

Orr Jr., C. (1969). *Application of mercury penetration to material analysis, powder technology*. Elsevier Sequoia S.A., Lausanne, Switzerland, 117–123.

Ouyang, C., Landis, E., and Shah, S. P. (1991). "Damage assessment in concrete using quantitative acoustic emission." *ASCE J. Engrg. Mech.*, ASCE, 117(11), 2681–2698.

Pyrak, L. J. (1988). "Seismic visibility of fractures," PhD thesis, Dept. of Mat. Sci. and Mineral Engrg., Univ. of California at Berkeley.

Regnault, P., and Bruhwiler, E. (1990). "Holographic interferometry for the determination of fracture process zone in concrete." *Engrg. Fracture Mech.*, 35(1–3), 29–38.

Scrivener, K. L., and Nemati, K. M. (1996). "The percolation of pore space in cement paste/aggregate interfacial zone of concrete." *Cement and Concrete Res.*, 26(1), 35–40.

Slate, F. O., and Olsefski, S. (1963). "X-rays for study of internal structure and microcracking of concrete." *J. ACI, Proc.*, 60(31), 575–588.

Whitehurst, E. A. (1966). "Evaluation of concrete properties from sonic tests." Monograph No. 2, American Concrete Institute, Detroit, Mich.

Yadev, G. D., Dullien, F. A. L., Chatzis, I., and Macdonald, I. F. (1984). "Microscopic distribution of wetting and non-wetting phases in sandstone during immiscible displacements." *Proc., 1984 SPE Annu. Tech. Conf. and Exhibition.*

Zheng, Z. (1989). "Compressive stress-induced microcracks in rocks and applications to seismic anisotropy and borehole stability," PhD thesis, Dept. of Mat. Sci. and Mineral Engrg., Univ. of California, Berkeley.